


Multiclass Classification of Cervical Pap Smear Images Using Deep Learning-Based Model

Krishna Prasad Battula, Bolem Sai Chandana* 

School of Computer Science and Engineering, VIT-AP University, Amaravati 522237, India

Corresponding Author Email: saichandana.blem@vitap.ac.in



<https://doi.org/10.18280/ts.400204>

ABSTRACT

Received: 7 November 2022

Accepted: 16 March 2023

Keywords:

cell segmentation, cervical cancer, features extraction, manual analysis, wrapper filter

One of the primary reasons for women's deaths is cervical cancer. The most important procedures that are to be performed to ensure the reduction of cervical cancer's side effects are possible diagnosis and the most definitive possible medical treatment. One of the best methods for identifying this type of cancer is using PaP smear images. For cervical cancer detection in PaP smear images, this research proposes a novel hybrid deep learning approach. The proposed methodology for cervical cancer classification performs the four efficient stages. A shape-based iterative method is used to detect nuclei in cell segmentation, and a marker-control watershed approach is used to separate overlapping cytoplasm. From the regions of segmented nuclei and cytoplasm, the practical features are extracted in the features extraction step. The simulated annealing integrated with a wrapper filter is employed for efficient feature selection. The classification of cervical cancer from pap-smear images is achieved using an attention-based nested classification network (Anu-Net) based on deep learning. The SIPaKMeD dataset is used for experiment analysis. The experimental results reveal that the developed deep-learning network model enabled high classification accuracy. The accuracy for a binary class problem was 99.95%; for a three-class problem was 99.98%; and a five-class problem was 99.74%. The proposed approach significantly outperformed existing deep learning models in binary class, three-class, and five-class problems than the existing approaches.

1. INTRODUCTION

The fourth most common cancer among women is cervical cancer, which develops in the woman's cervix [1]. The World Health Organization (WHO) reports that 311 000 women died from cervical cancer in 2018 alone, with an estimated 570 000 women worldwide receiving a diagnosis [2]. Due to a lack of screening and treatment facilities, developed and underdeveloped countries account for more than 80% of instances of cervical cancer and 85% of fatalities from the disease [3]. The main risk factors for human papillomavirus (HPV) infection include smoking, early pregnancy, poor menstrual hygiene, and the use of oral preventatives [4]. The primary cause of cervical cancer is a long-term HPV infection, according to research [5]. However, if diagnosed early and given the proper care, the most treatable malignancy is cervical cancer [6].

Over 30 years old, cervical cancer diagnoses are made possible by women's routine screening, which is essential to preventing the disease [7]. Cervical malignancies are identified using cervical cytopathology (pap smear test); this screening technique is the most popular due to its affordability [8]. The malignancy is examined by extracting the cells from the cervix squamocolumnar terminal using a light microscope [9]. A single slide typically requires 5 to 10 minutes to analyze due to the cells' varying orientations and overlaps [10]. Each slide comprises over three million cells with varied directions and overlaps, making the human screening process laborious, repetitive, expensive, and prone to errors. As a result, a

developed system that can accurately and effectively evaluate the pap cell is being developed [11].

The computer-aided diagnostic (CAD) system developed to assist medical professionals in monitoring cervical cancer has attracted much interest [12]. Cell segmentation (cytoplasm and nuclei), feature extraction, and classification are the three phases of the typical CAD system [13]. To improve the quality of the images, the system uses filtering-based pre-processing operations [14]. Then, cell nuclei are extracted. After that, the segmented nucleus is corrected through post-processing [15]. The segmented nucleus is then used to extract handcrafted features like texture, color metric, and morphological characteristics [16]. The most discriminating features are then determined using the feature selection technique, and lastly, the cell classification is performed using a network model [17].

Processing the data using the technique mentioned above involves several steps, and the extracted handcrafted features cannot guarantee superior classification performance. This also demonstrates the limitation of automated learning [18]. Deep learning-based feature extraction techniques outperform other machine learning (ML) algorithms to obtain an improved CAD system. The existing model's outcomes on complex tumor detection problems are being attained by DL-based algorithms [19]. One drawback of deep learning is that, in comparison to ML techniques, it requires more data to provide effective results, which is challenging to acquire in the medical field. Additionally, deep learning could perform better for multiple classifications, which is quite common in the medical industry and has a disparity in sample data distribution.

Therefore, additional research and development are needed to analyze pap cells [20].

To effectively classify the cervical cytopathology cell, we have developed the Attention-based nested U-Net (Anu-Net) model based on deep learning in this research. To test the proposed model, the SIPAKMED dataset is used. The proposed methods outperformed the existing models.

The main contributions of the research are

- First, we performed image pre-processing to enhance the performance of classification and segmentation. Image enhancement and noise removal processes are performed in the image pre-processing stage. The gaussian filter removes noise in the image, and CLAHE (contrast limited adaptive histogram equalization) is used to enhance the image contrast.
- Following Nuclei and cytoplasm of the image are segmented. A shape-based iterative technique is used to segment nuclei, and the marker-controlled watershed technique is used to segment overlapping cytoplasm.
- After that, the significant relative features of the disease are then extracted. The optimum features are selected using simulated annealing integrated with a wrapper filter.
- Finally, the multiple cervical cancer classifications are classified using deep learning-based Anu-Net. The more effective performance is attained by the proposed model using the SIPAKMED dataset. It demonstrates the possibility of improving cervical cancer detection methods.

The rest of this paper has been divided into the following sections: The most current studies employing deep learning approaches for detecting and forecasting cervical cancer are discussed in Section 2. Section 3 provides the proposed methodology, which describes the overall workflow of the research. Afterward, Section 4 discusses the result and analysis. Finally, Section 5 provides the conclusion of the study.

2. RELATED WORKS

This section reviews some existing DL techniques for cervical cancer classification and segmentation.

For cervical cancer detection, two deep-learning network models are proposed by Chandran et al. [21] using colposcopy images. Cervical cancer is detected by using CYENET and VGG19 models in this research. The transfer learning approach is used for training the VGG19 in CNN architecture.

For the early detection of cervical cancer, the novel MASO-optimized DenseNet 121 model is proposed by Chitra et al. [22] in this paper. The training samples are initially increased by applying various augmentation techniques, including vertical flip, horizontal flip, shearing, zooming, width shift, height shift, brightness, and rotation. The hyperparameters are optimized by using the effective optimization algorithm.

For the automatic detection and classification of cervical cancer, a fully-automated pipeline is proposed by Alyafeai and Ghouti [23] in this research. The cervical tumor is detected and classified using two lightweight CNN models in the proposed model. The cervix tumors are classified by the second model using self-extracted features.

For image regeneration and cervical data classification, a hybrid variational Convolutional (CNN) autoencoder network is proposed by Khamparia et al. [24]. Convolution functions as the encoding stage of the models. The autoencoders are used for handling the decoding phase. The damaged tissue or

malignant cells are regenerated by using autoencoders. The convolutional model with useful features was used for generating high-dimensional feature vectors in the encoding end. The variational autoencoders are used for reconstructing these high-dimensional feature vectors.

For cervical cancer classification, an ensemble model based on deep learning is proposed by Diniz et al. [25] using CNN. The development of a decision-support tool for cytopathologists depends heavily on this work. The nuclei are segmented by using this tool. A more accurate model was created using cross-validation, dropout, and data augmentation techniques.

Using pre-trained CNN algorithms, a CPS image model for a single cell is presented by Mohammed et al. [26] in this research. The image classification model of the chosen DCNN is employed for detailed experiment analysis.

The combined image segmentation and classification model is proposed by Desiani et al. [27] in this research. The image quality is increased by using CLAHE before segmentation. In the proposed model, the CNN model performs the segmentation.

The existing papers on pap smear image classification have more drawbacks, such as (i) Requiring high computing resources for training on high-resolution data. (ii) It reduces the recognition rate for classification, (iii) It reduces the quality of classifiers in real-time applications, (iv) Most of the existing deep learning models will decrease their classification accuracy in cases where the number of classes is very high, and (v) It does not perform well in real-time applications. We propose a new deep learning-based Anu-Net model for the reliable classification of cervical cancer diseases for solving these challenges.

3. PROPOSED METHODOLOGY

The proposed deep learning-based cervical cancer classification model is shown in Figure 1. The proposed model's main steps are acquiring the image, image pre-processing, segmenting cell components, and image classification. The SIPaKMeD dataset is utilized during the image acquisition stage for multi-cells. The image quality is improved by enhancing and denoising the input pap smear images as an image pre-processing stage. Cell segmentation is the next stage. This step divided the input images into exciting areas, such as the nucleus and cytoplasm. The subsequent phase was feature extraction after segmentation. Distinct significant regions or features are extracted during feature extraction. The optimum features are selected by employing simulated annealing integrated with a wrapper filter. Classification of cervical cancer is the last step. A deep learning-based Anu-Net is used for classifying normal and abnormal cells at this stage. Each subsection has a description of each phase.

3.1 Image acquisition

SIPaKMeD recently released an accessible dataset, which is used in this research. The 966 full slide pap smear images are included in the database and manually cropped into 4049 single-cell pictures. The cells were divided into five classes according to their level of abnormalities benignity - parabasal cells (PC), superficial-intermediate cells (SIC), dyskeratotic cells (DC), koilocytotic cells (KC), and metaplastic cells (MC).

The initial two are healthy, the next two are abnormal, and the final is benign. There appears to be a uniform image distribution among the single-cell image classes (831, 787, 825, 793, and 813, respectively). Table 1 includes a description of the dataset's details.

3.2 Image enhancement

Noises or other artifacts may be present in the pap smear images. Images from pap smears may have worse quality due to noise or contrast. Deleting noises and enhancing the image's quality in cell contrast is necessary. The noise is removed by using a Gaussian filter. The cell contrast is improved by using CLAHE. The input cell images, grayscale images, and pre-processed images for all classes are shown in Figure 2.

Table 1. Sipakmed (multi-cells) dataset five-class cell descriptions

Class	Total Images	Total Cells
Normal Cells		
1. Parabasal cells	108	787
2. Superficial-Intermediate cells	126	831
Abnormal Cells		
3. Koilocytotic cells	238	825
4. Dyskeratotic cells	223	813
Benign Cells		
5. Metaplastic cells	271	793
Total	966	4049

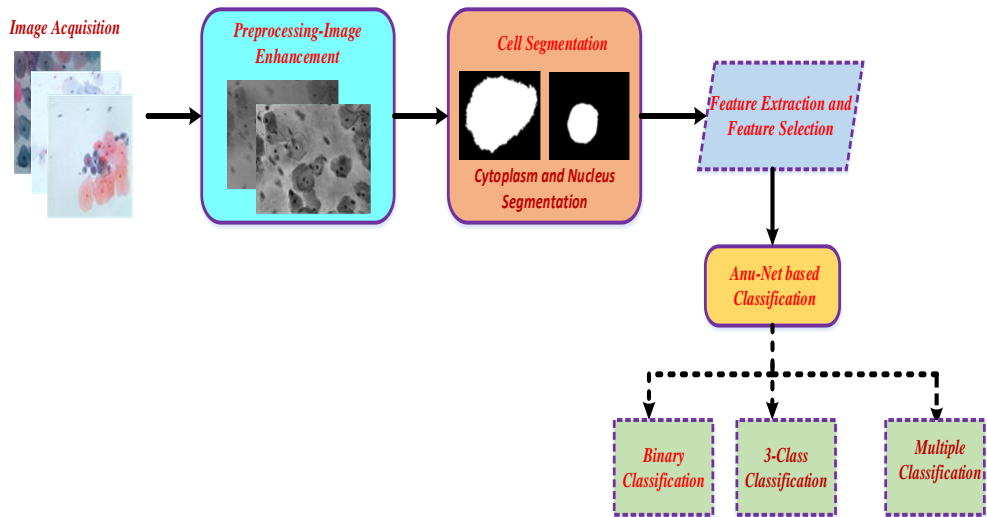


Figure 1. Schematic structure of the proposed methodology

Classes	Input Image	Grayscale Image	Noise Removal	Image Enhancement
DC				
KC				
PC				
MC				
SIC				

Figure 2. Pre-processing results for classification and segmentation

3.3 Segmentation of cytoplasm and nuclei

From each segmented cell, this stage involved the segmentation of the nuclei and cytoplasm that had emerged from the segmentation of overlapping cells. The segmentation stage of overlapping cells produced three different types of segmented cells. The cells were isolated, overlapping, and touching. Three separate sub-processes were established for the segmentation of the nucleus and cytoplasm. Segmenting the cell components from isolated cells is the first process. Segmenting the cell components from touching cells is the second process. Segmenting the cell components from overlapping cells is the last process. The results of the watershed transform technique for segmented cells could be used to extract the cytoplasm boundary of overlapping, touching, and isolated cells. It was suggested during the segmentation process for the overlapping cells. The image obtained during the segmentation did not contain enough touching patches and overlapping cytoplasm to depict the cytoplasm boundaries accurately. Therefore, we applied an edge-smoothing technique to smooth the cytoplasm boundaries.

Edges smoothing method's processing steps

- Grayscale image reading and binary image conversion
- Extracting only the most enormous blob
- Crop the top and left of the frame
- Fill holes
- Blurring the image
- Threshold again
- Display the smoothed binary image using the smoothing method

The shape-based iteration technique described below was used to segment the nuclei of overlapping, touching, and isolated cells.

Shape-based nuclei detection algorithm's processing steps

- Input color image reading and convert a grayscale image
- Using a Gaussian filter to remove noise

- Predefining the values of solidity, minimum and maximum intensity values, major and minor axis lengths, and minimum area
- Image binarizing using the highest and lowest thresholds.
- Removing the limited intensity and shape value regions
- Segmenting nuclei

Segmenting the nuclei was simpler than segmenting the cytoplasm. The nuclei in the image of multiple cells have effective qualities, such as the shapes are usually circular or oval and well-structured and low intensity. In the other regions, like cytoplasm or background, the nuclei are considerably different. The most significant characteristics of nuclei used for differentiating the background and cytoplasm are solidity, major and minor axis lengths, average intensity, and area. The nuclei are segmented and detected by developing the method based on these characteristics.

The original Pap smear images are processed with a Gaussian filter to eliminate the noise. The nuclei segmentation process uses shape-based features (solidity, minor axis length, significant axis length, intensity values, and area). The experiments showed that the smallest nucleus size was $362 \mu\text{m}^2$. The solidity values were less than or equal to 0.98, and between 60 and 150 was the average intensity value. The length of the minor axis varied from 17 to 87 meters, whereas the size of the main axis for nuclei ranged from 24m to 117m.

Figures 3 and 4 demonstrate the results of the nuclei segmentation process. The effectiveness of nuclei detection using the proposed model is provided in Table 6. Tables 3-5 reveal the performance of segmentation, cytoplasm, and nuclei of isolated, overlapping, and touching cells. The segmentation for overlapping cells is tested on 4049 cytoplasm images. Isolating cells comprised 6.47% of the cytoplasm. In contrast, touching cells consisting 35.27% of the cytoplasm, and overlapping cells comprised 58.26% of the cytoplasm. Table 2 displays the overall segmented cytoplasm range and the percentage of segmented cytoplasm.

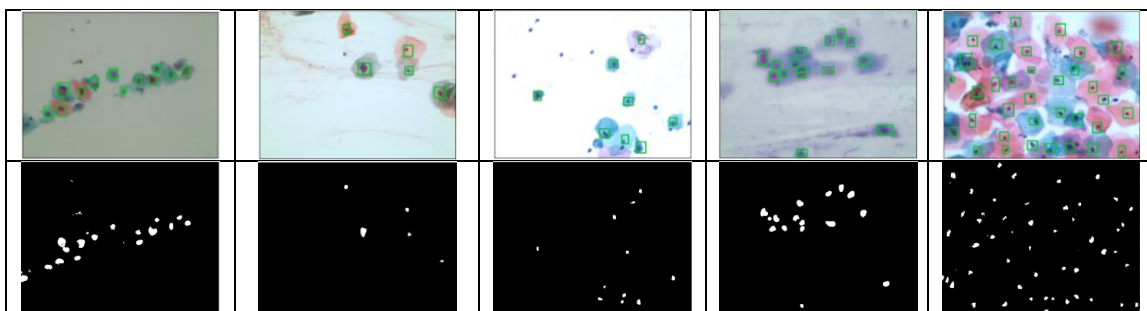


Figure 3. Detecting nuclei in Pap smear images of multiple cells

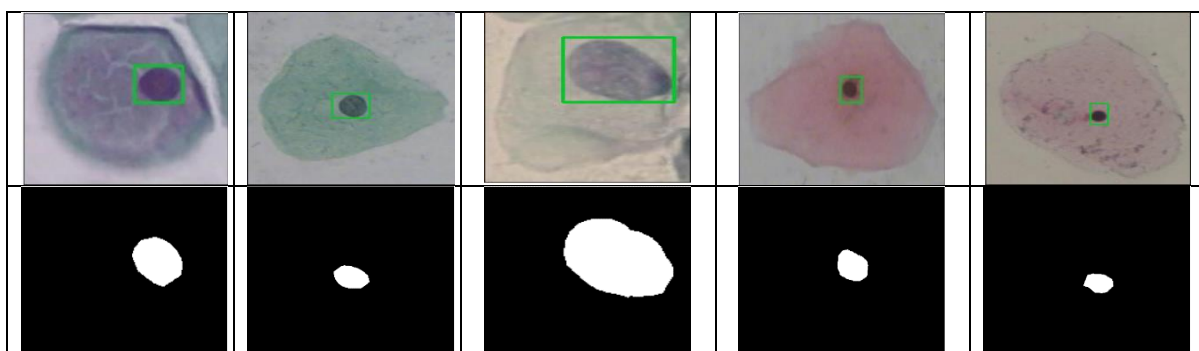


Figure 4. Detecting nuclei by cropping regions from single cells

Table 2. The percentage of cytoplasm that is well-segmented with the total number of cytoplasm

Overlapping Cytoplasm	Touching Cytoplasm	Isolated Cytoplasm	Total
2359	1428	262	4049
77.59%	95.85%	100%	95.94%

Table 3. Segmentation of cytoplasm and nuclei for isolated cells

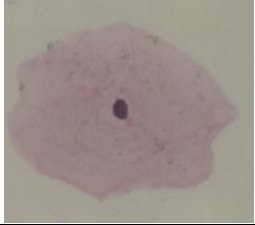


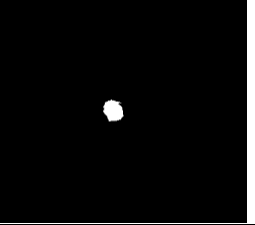
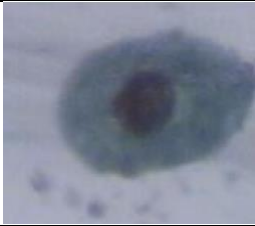

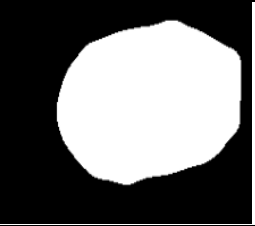
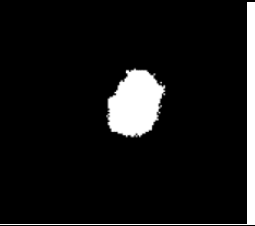
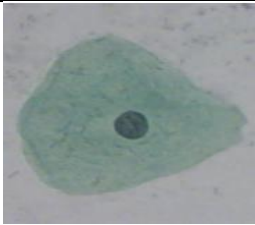


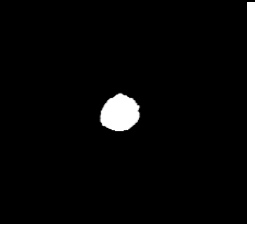
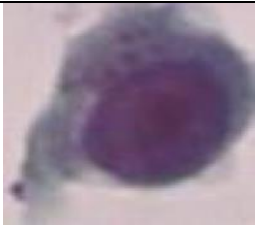



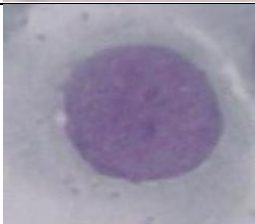
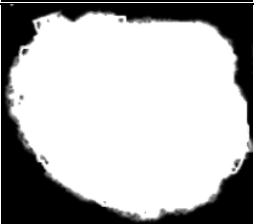
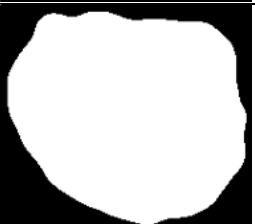
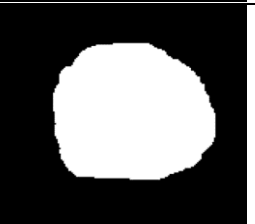
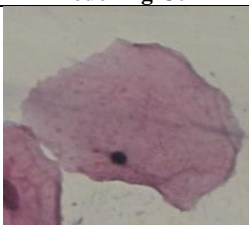


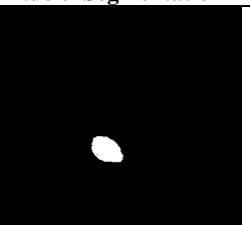
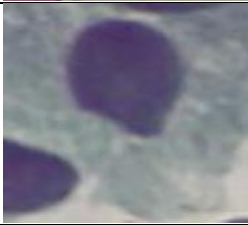
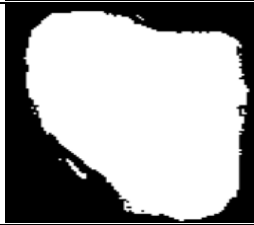
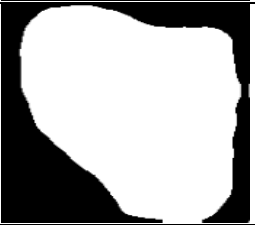
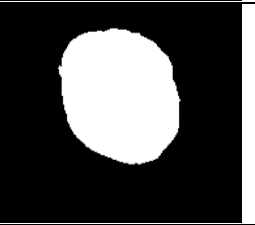
Class	Isolated Cell	Cytoplasm Segmentation	Smooth Boundary	Nuclei Segmentation
SIC				
PC				
MC				
DC				
KC				

Table 4. Segmentation of cytoplasm and nuclei for touching cells

Class	Touching Cell	Cytoplasm Segmentation	Smooth Boundary	Nuclei Segmentation
SIC				
PC				

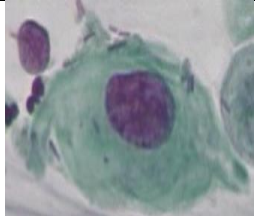






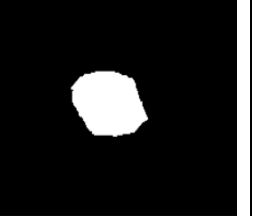


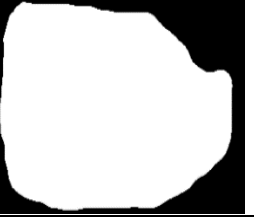




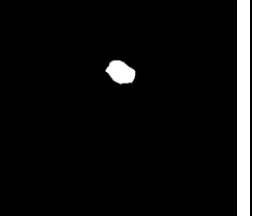







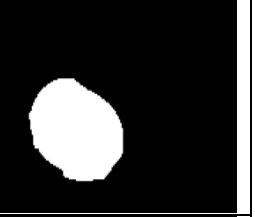



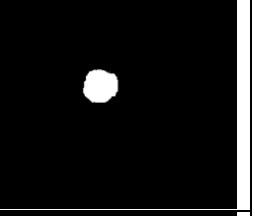
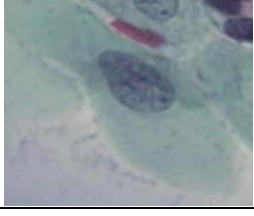



MC				
DC				
KC				

Table 5. Segmentation of cytoplasm and nuclei for overlapping cells

CLASS	Overlapping Cell	Cytoplasm Segmentation	Smooth Boundary	Nuclei Segmentation
SIC				
PC				
MC				
DC				
KC				

3.4 Features extraction

Feature extraction is the next stage after the cell segmentation stage. The cytoplasm and nucleus' essential features, such as color, shape, and texture, are now retrieved. The gray-level co-occurrence matrix (GLCM) algorithm extracts the disease's significant texture features. In a cervical pap smear image, the distribution of color and shape of abnormal and normal cells is very different. The morphology features are also extracted. Twenty-nine features are extracted from the nucleus due to the biological importance of the nucleus in the classification of cancer. The features include six texture features (entropy, energy, smoothness, variance, mean, and standard deviation) and three additional geometric features (eccentricity, compactness, and solidity).

3.4.1 GLCM features

The energy features of the cervical image are extracted using the GLCM feature extraction technique. One can be constructed for any single-channel image. A square matrix constitutes the GLCM. An equal range of columns and rows is present in the grayscale of the original image. In the fused cervical image, the GLCM matrix is generated by counting different orientations' grayscale intensity pixels. This work uses a 45° angle to build the GLCM matrix. From the healthy cervical image, the cancerous image is distinguished using GLCM features like correlation, entropy, energy, and contrast.

Correlation:

R calculates the relationship between adjacent pixels' brightness. Row average represents 'i', and column average represents 'j' for GLCM.

$$Correlation(R) = \sum(i - \mu_i)(j - \mu_j) \frac{p(i, j)}{[\sigma_i \sigma_j]} \quad (1)$$

Contrast: The grayscale difference between two adjacent pixels is calculated by this texture feature.

$$Contrast = \sum(|i - j|^2 \times p(i, j)) \quad (2)$$

Entropy: This metric measures the proximity of the GLCM elements to the diagonal. The value ranges from 0 to 1, which is defined as,

$$Entropy = -\sum p(i, j)[\log_2 p(i, j)] \quad (3)$$

Energy: For all the GLCM components, the squares are added to determine the second angular moment.

$$Energy(E) = \sum p(i, j)^2 \quad (4)$$

For an image, the range of the homogeneity unit of measurement, called energy, is zero to unity.

3.4.2 Morphological features

The morphological properties are determined by cell size and shape. The morphological properties of cells are ascertained for this investigation using eight connected chain codes. The eight corresponding pixels are those that surround the eight-linked chain code. The nucleus-to-cytoplasm ratio is defined as,

$$\frac{N}{C} = \frac{Nucl_{area}}{Nucl_{area} + Cyto_{area}} \quad (5)$$

3.5 Features selection

Selecting the extracted feature subsets that produce better classification results is a feature selection technique. Some of the collected features contain noise, and the network model will not select these features for classification. Consequently, it is necessary to identify the optimum set of features by exploring all possible combinations. The algorithm's computational complexity is increased when using multiple features; the number of possible combinations explodes. The filter, wrapper, and embedding approaches are general classifications for feature selection algorithms.

Simulated annealing with a wrapper approach is combined in the proposed method. A double-strategy random forest technique is used in this research to assess the performance of the feature selection, although this method has already been proposed. The probabilistic method of "simulated annealing" can be used to approximate a function's global optimum. The technique works well to ensure that the best combination of features is chosen. The below algorithm shows the steps of the simulated annealing approach.

Begin simulated annealing

S = Select starting point (typically around 0.2)

I = number of iterations

BF = all features (Backward selection)

Actual error = Error (BF)

For I=1 to Maximum iterations

I=I-1

Randomly select to add or remove a feature to BF

New error=Error (BF)

If($e((\text{Actual error}-\text{New error})/S) > \text{rand}[0 \dots 1]$)

Accept and keep the new features in BF

Actual error=New error

Else

Keep the old features

End if

End for

End

A fitness value serves as the direction for choosing the desired set. The fittest (i.e., the one that performs the best) feature subset is selected after all the simulated annealing subsets have been compared. A wrapper is utilized to acquire the fitness value search, and the classification algorithm's error was calculated using k-fold cross-validation. The retrieved traits are combined into various combinations, then created, assessed, and contrasted with other varieties. The evaluation of a set of features is then done using a prediction model, and a score is given according to the model's accuracy.

3.6 Classification using anu-net

A model's classification phase finally ends with the desired result of predicting the label. We classified the input image using the multiclass classification algorithm according to the selected features in the proposed approach. From pap smear images, cervical cancer is classified using the Anu-Net model in this research.

We develop an ANU-Net integrated network based on the Attention mechanism and Nested U-Net architecture to classify medical images. Figure 5 provides a framework for ANU-Net. The primary network framework ANU-Net uses is nested U-Net, as can be seen, and decoders and encoders are equally organized on both sides of the network. Dense skip connections are used to transfer the reliable data obtained by

the encoder to the decoder of the relevant layers, allowing for the extraction of hierarchical features that are more effective.

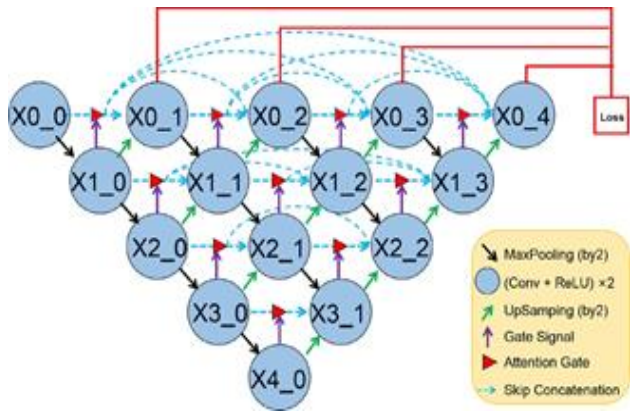


Figure 5. Structure of ANU-Net

The two equal-scale feature maps are received by each decoder's convolution block as inputs when there are dense skip connections: (1) Using previous Attention Gate outputs coupled with a same depth skip connection, the intermediate feature maps are produced; (2) The result of the more profound block deconvolution operation is the final feature map. The decoder then reconstructs features from the bottom up after receiving and concatenating all feature maps. Earlier nested convolution block's feature maps in this layer accumulate and reach the present block because dense skip connections can fully utilize these feature maps.

The feature map is defined as follows, let the convolution block output is represented by $Q_{u,v}$, where the network's feature depth is represented by u , and the sequence of the convolution blocks along the skip connections in the u th layer is depicted by v ; consequently, the retrieved feature map equation is defined as,

$$Q_{u,v} = \left\{ \begin{array}{l} \phi[Q_{u-1,v}] \\ \phi \left[\sum_{k=0}^{v-1} Ag(Q_{u,k}) U_P(Q_{u+1,v-1}) \right] \end{array} \right. \quad , v = 0 \quad (6)$$

where, the convolution block followed by concatenation merger is denoted by $\phi[\]$. The attention gate selection and mean upsampling are represented by $Ag(\)$ and $U_P(\)$. Concatenating the Attention Gates' output results from a node $Q_{u,k=0}$ to $Q_{u,k=v-1}$ in the u th layer is indicated by $\sum_{k=0}^{v-1} Ag(Q_{u,k})$.

In the first layer, the process of feature maps traveling through the skip connection is detailed in Eq. (6).

As an illustration, a block $Q_{0,4}$ possesses five inputs. The first four are the previous v block outputs in this layer, and the remaining input is the second layer's upsampling feature from a block $Q_{1,3}$. ANU-Net's most significant innovations are: Dense skip connections were used in the network transfer to integrate hierarchical representations utilizing the quality that the encoder had retrieved. In the decoder path, the features retrieved at various levels are combined by implementing the Attention Gate between layered convolution blocks with a focused selection.

4. EXPERIMENTAL RESULTS

This section describes the experimental datasets, environment settings, and software and hardware

requirements. Furthermore, both the performance analysis and evaluation criteria are well-explained.

4.1 Data setting

In each class, the proposed model is trained by using 60% of the dataset, validation is done by 20%, and testing is performed by using 20%. The implementation is performed by binary class (Normal and abnormal), ternary class (Normal, abnormal, and benign), and multiple types (dyskeratotic, metaplastic, parabasal, superficial, and koilocytotic) of the dataset. Moreover, A factor of 6 is added to the training dataset due to the implementation of training set data augmentation techniques. Table 6 displays the final training, validation, and test dataset. The performance is done by using the python platform.

Table 6. The SIPAKMED dataset's experimental data setup

Dataset	Total Number of Images		
	2-Class	3-Class	5-Class
Training	13664	16989	16982
Validation	652	811	811
Test	652	811	812

4.2 Evaluation metrics

Choosing an appropriate evaluation metric is essential to overcoming bias among the various algorithms. The most common metrics for assessing classification performance are F1 score, recall, precision, and accuracy. Precision is defined as the proportion of appropriately detected samples over all recognized representations. A classification model's ability to identify each relevant sample is described by the recall. Using the harmonic mean, the precision and recall metrics are combined with the F1 score. According to the definition of accuracy, it is the percentage of properly predicted samples out of all samples. Table 7 displays the evaluation measure's mathematical formulations. In Table 7, precisely counted negative samples that were obtained are known as the "True Negative" (TN), the number of correctly labeled positive samples is known as the True Positive (TP), and the False negative (FN) represents the number of positive instances predicted as negative, False positive (FP) represents the number of negative samples classified as positive.

Table 7. Evaluation measures

Calculations	Prescription
Accuracy	$\frac{TP+TN}{TP+TN+FP+FN}$
Precision, P	$\frac{TP}{TP+FP}$
Recall, R	$\frac{TP}{TP+FN}$
F1 score	$2 \times \frac{P \times R}{P+R}$

4.3 Evaluation results

The performance of the classification of cervical tumors is examined for problems with binary class, three-class, and five-class classification. The pap smear images are effectively classified by the proposed model. For the proposed model, the performance of types is explained by the confusion matrices. With fewer misclassifications, this model performed admirably across all classes.

4.3.1 Binary classification

In this case, the proposed model classified normal and abnormal cervical cells. We offer confusion matrices of the proposed Anu-Net model to demonstrate the classification performance. For binary classification, the confusion matrix is shown in Figure 6. Although one regular image is classified as abnormal, the proposed model's binary type correctly identifies 323 images as normal and 328 as abnormal. It is recognized that for binary classification problems, the proposed model produced significantly very high accuracy.

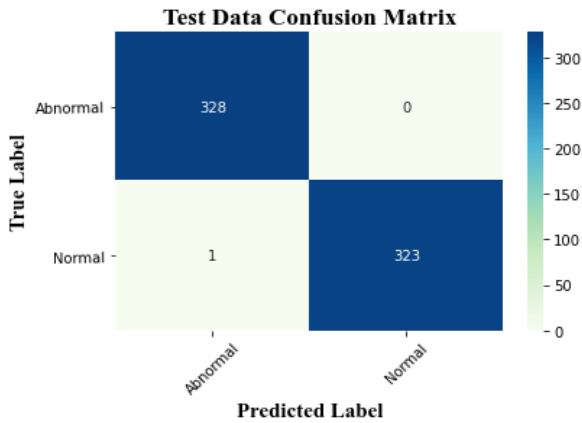


Figure 6. Confusion matrix for binary classification

The performance comparison of the proposed model with the existing deep learning models for binary classification is given in Table 8. Figure 7 shows the performance comparison for binary type. Compared to the existing model, the proposed model successfully classifies between normal and abnormal images. The highest classification results are obtained by the proposed model with overall accuracy (99.95%), precision (99.97%), recall (99.87), and F1 score (99.98). Classification accuracy is 99.38% and 98.77% for the ResNet-50 and VGG19, respectively. The least accurate performance is achieved by EfficientNet-B0, which performs at 95.03% overall.

Table 8. Performance evaluation for binary classification

CNN Models	Accuracy (%)	Precision (%)	Recall (%)	F1-Score (%)
EfficientNet-B0	95.03	94.98	95.24	95.04
VGG-19	98.77	98.52	95.45	98.78
XceptionNet	98.31	98.82	98.02	99.54
ResNet-50	99.38	99.64	98.56	99.24
HDFFF	99.85	99.86	99.64	99.93
Proposed Model (Anu-Net)	99.95	99.97	99.87	99.98

4.3.2 Ternary (3-Class) classification

The proposed model divided the cervical cells for ternary categorization into normal, abnormal, and benign. Figure 8 displays the confusion matrix for ternary classification. The confusion matrix demonstrates that the proposed approach incorrectly identifies only five images, which correctly classifies 324 images as normal, 326 images as abnormal, and 156 images as benign. From the confusion matrix, the performance results of the proposed model effectively classify the normal, abnormal, and benign images.

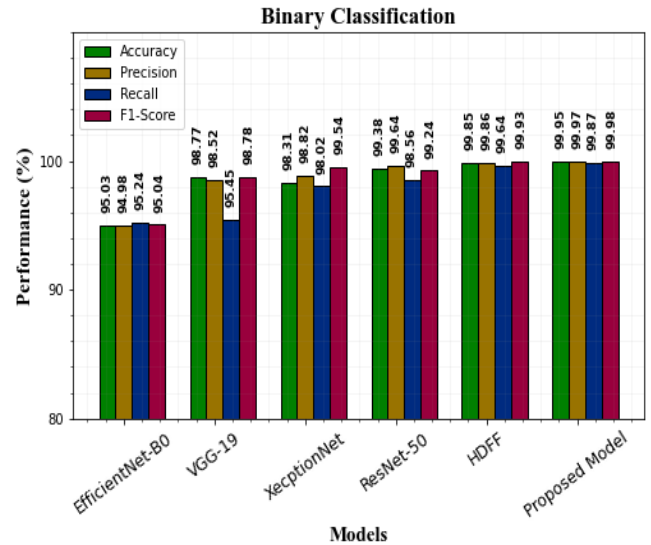


Figure 7. Performance comparison for binary classification

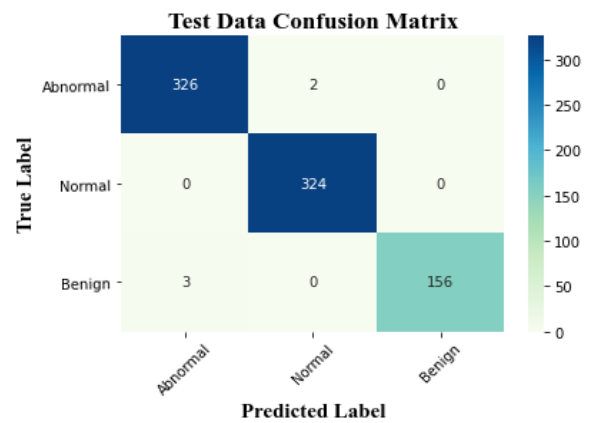


Figure 8. Confusion matrix for ternary classification

The performance comparison of the proposed model with the existing deep learning models for ternary classification is given in Table 9. Figure 9 shows the Performance Comparison for 3-class classification. The VGG16 achieves 97.90% classification accuracy with an average F1-score (97.32%), recall (97.02%), and precision (97.60%). The average F1 score, recall, and precision for VGG19 and ResNet-50 are 96.18%, 95.21%, and 96.30%, respectively. 96.18% accuracy is achieved by both of them. But, the worst performance is produced by XceptionNet and contributes with an accuracy rate of 89.64%. Better classification accuracy of 99.98% is achieved by the proposed Anu-Net model with an F1 score (99.89%), recall (99.92%), and precision (99.85%).

Table 9. Performance evaluation for ternary classification

CNN Models	Accuracy (%)	Precision (%)	Recall (%)	F1-Score (%)
XceptionNet	89.64	92.02	96.32	95.60
ResNet-50	96.18	96.30	95.21	96.18
VGG19	96.18	96.30	94.43	96.18
VGG16	97.90	97.60	97.02	97.32
HDFFF	99.38	99.32	99.34	99.38
Proposed Model (Anu-Net)	99.98	99.85	99.92	99.89

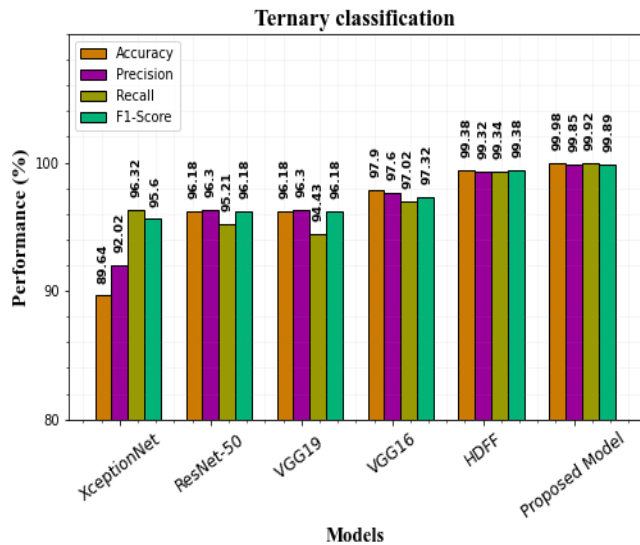


Figure 9. Performance comparison for 3-class classification

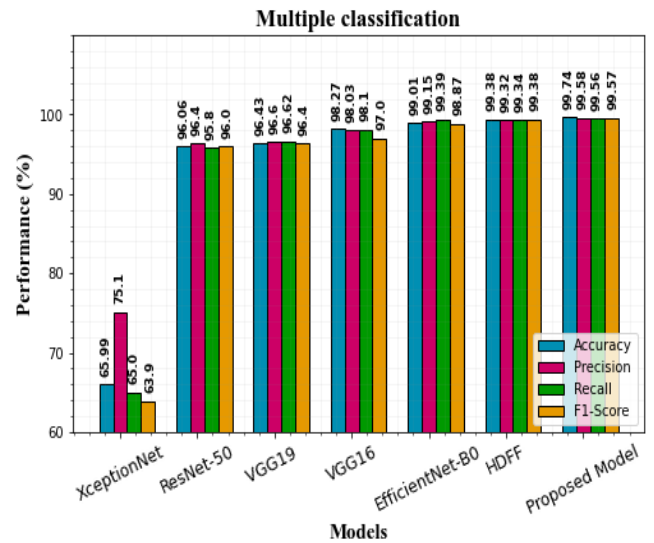


Figure 11. Performance comparison for multiple (5-class) classifications

4.3.3 Multiple (5-Class) classification

The cervical cells are classified into five classes for this experiment. Class 1 cells are superficial intermediate cells, Class 2 cells are parabasal cells, Class 3 cells are metaplastic, Class 4 cells are dyskeratotic cells, and Class 5 cells (are koilocytotic cells). The proposed Anu-Net model's confusion matrices for multiclass classification are displayed in Figure 10. Out of 812 images, 805 are correctly classified using the proposed model for the 5-class type. The effectiveness of the proposed model efficiently classifies the multi-classification problems.

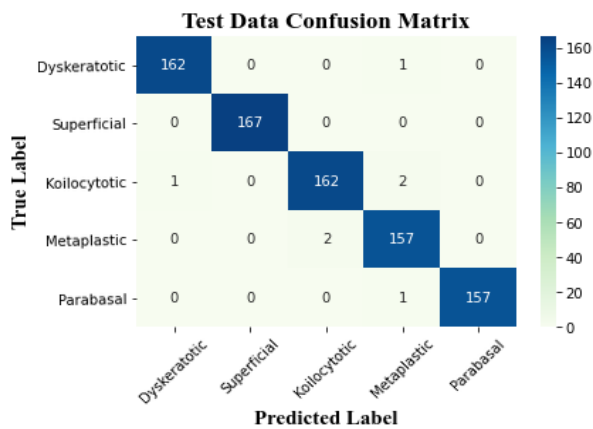


Figure 10. The confusion matrix of the proposed model for the 5-class classification problem

Table 10. Performance evaluation for multiple classifications

CNN Models	Accuracy (%)	Precision (%)	Recall (%)	F1-Score (%)
XceptionNet	65.99	75.10	65.00	63.90
ResNet-50	96.06	96.40	95.80	96.00
VGG19	96.43	96.60	96.62	96.40
VGG16	98.27	98.03	98.10	97.00
EfficientNet-B0	99.01	99.15	99.39	98.87
HDFF	99.38	99.32	99.34	99.38
Proposed Model (Anu-Net)	99.74	99.58	99.56	99.57

4.3.4 Performance comparison results

Using the SIPAKMED dataset for classifying the cervical cells, a comparative performance analysis of the proposed Anu-Net model with existing works is presented in Table 11. For multiclass and binary classification problems, the proposed model achieved high classification accuracies from table recognition. Individual existing model's overall accuracy declines as the number of classes increases, but the proposed deep learning-based Anu-Net model performs well. The proposed strategy outperformed the current studies for 5-class and binary classification tasks, respectively, with accuracy gains of 1.70 and 0.28 percent. In previous studies, it has been observed that no solution has been discovered for the 3-class classification problem.

Table 11. Classification accuracy comparison using the SIPAKMED dataset

Ref	Method	Class	Accuracy (%)
[28]	CNN Graph	2-Class	99.70
[29]	convolutional Network	5-Class	98.37
[30]	DenseNet-161	5-Class	98.96
[31]	Bagging Ensemble classifier	2-Class	98.25
		5-Class	94.09
Proposed Model	Anu-Net	5-Class	99.74
		3-Class	99.98
		2-Class	99.95

The better results are achieved by conducting the training phase with 26 epochs and a learning rate of 0.01. For each epoch, the experiment analysis used 31 iterations. The training and validation accuracy and loss graph for multiple cervical cancer classifications is given in Figure 12. With an accuracy of 99.89%, training progress validation was performed. Three seconds per epoch are needed for the computations necessary to train the proposed model. 2.5 seconds are taken for testing the proposed model for classification.

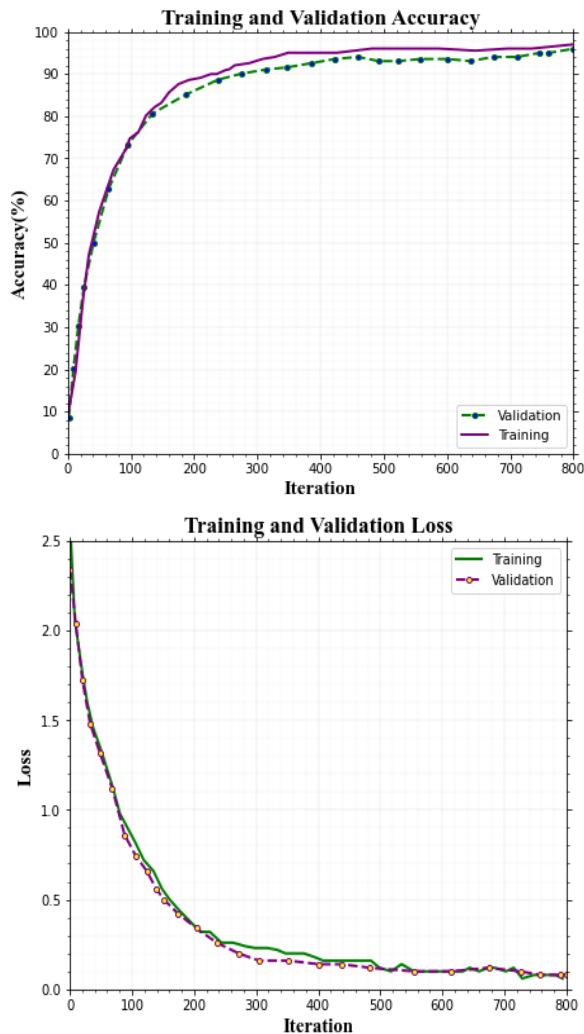


Figure 12. The training and validation performance (accuracy and loss) of the multiclass classification of cervical cancer

5. CONCLUSION

For cervical cancer classification, a new deep learning-based Anu-Net model is proposed in this research using Pap smear images. The nucleus and cytoplasm of each independent cell component are first segmented by the proposed model. Then a deep learning-based methodology was used to determine whether or not the cells were cancer. There are many methods have been developed in this direction in the past. However, it has not been discovered to be very accessible for accuracy.

The proposed model with selected useful features achieved a classification accuracy of 99.95% for a binary class problem, 99.98% for three class problems, and 99.74% for multiple

classification problems in this paper. The overall classification performance is increased by the proposed model in classifying the abnormal cells from the normal ones. The proposed system outperforms other well-known deep learning network models in classification accuracy. The cervical cancer screening system detects malignancies early by using the proposed framework. We intend to incorporate an assessment of the risk factors for cervical cancer into the proposed model in further research.

AUTHORS' CONTRIBUTIONS

The author confirms sole responsibility for the following: study conception and design, data collection, analysis and interpretation of results, and manuscript preparation.

REFERENCES

- [1] Khamparia, A., Gupta, D., de Albuquerque, V.H.C., Sangaiah, A.K., Jhaveri, R.H. (2020). Internet of health things-driven deep learning system for detection and classification of cervical cells using transfer learning. *The Journal of Supercomputing*, 76: 8590-8608. <https://doi.org/10.1007/s11227-020-03159-4>
- [2] Taha, B., Dias, J., Werghi, N. (2017). Classification of cervical-cancer using pap-smear images: A convolutional neural network approach. In: Valdés Hernández, M., González-Castro, V. (eds) *Medical Image Understanding and Analysis. MIUA 2017. Communications in Computer and Information Science*, vol 723. Springer, Cham. https://doi.org/10.1007/978-3-319-60964-5_23
- [3] Wentzensen, N., Lahrmann, B., Clarke, M.A., et al. (2021). Accuracy and efficiency of deep-learning-based automation of dual stain cytology in cervical Cancer screening. *JNCI: Journal of the National Cancer Institute*, 113(1): 72-79. <https://doi.org/10.1093/jnci/djaa066>
- [4] Chen, H., Liu, J., Wen, Q.M., Zuo, Z.Q., Liu, J.S., Feng, J., Pang, B.C., Xiao, D. (2021). CytoBrain: Cervical cancer screening system based on deep learning technology. *Journal of Computer Science and Technology*, 36: 347-360. <https://doi.org/10.1007/s11390-021-0849-3>
- [5] Gupta, S., Gupta, M.K. (2022). Computational prediction of cervical cancer diagnosis using ensemble-based classification algorithm. *The Computer Journal*, 65(6): 1527-1539. <https://doi.org/10.1093/comjnl/bxaa198>
- [6] Mohammadi, R., Shokatian, I., Salehi, M., Arabi, H., Shiri, I., Zaidi, H. (2021). Deep learning-based auto-segmentation of organs at risk in high-dose rate brachytherapy of cervical cancer. *Radiotherapy and Oncology*, 159: 231-240. <https://doi.org/10.1016/j.radonc.2021.03.030>
- [7] Guo, P., Singh, S., Xue, Z., Long, R., Antani, S. (2019). Deep learning for assessing image focus for automated cervical cancer screening. In *2019 IEEE EMBS International Conference on Biomedical & Health Informatics (BHI)*, Chicago, IL, USA, pp. 1-4. <https://doi.org/10.1109/BHI.2019.8834495>
- [8] AlMubarak, H.A., Stanley, J., Guo, P., et al. (2019). A hybrid deep learning and handcrafted feature approach for cervical cancer digital histology image classification.

- International Journal of Healthcare Information Systems and Informatics (IJHISI), 14(2): 66-87. <https://doi.org/10.4018/IJHISI.2019040105>
- [9] Allehaibi, K.H.S., Nugroho, L.E., Lazuardi, L., Prabuwo, A.S., Mantoro, T. (2019). Segmentation and classification of cervical cells using deep learning. *IEEE Access*, 7: 116925-116941. <https://doi.org/10.1109/ACCESS.2019.2936017>
- [10] Zahras, D., Rustam, Z. (2018). Cervical cancer risk classification based on deep convolutional neural network. In 2018 International Conference on Applied Information Technology and Innovation (ICAITI), Padang, Indonesia, pp. 149-153. <https://doi.org/10.1109/ICAITI.2018.8686767>
- [11] Yuan, C., Yao, Y., Cheng, B., Cheng, Y., Li, Y., Li, Y., Liu, X., Cheng, X., Xie, X., Wu, J., Wang, X., Lu, W. (2020). The application of deep learning based diagnostic system to cervical squamous intraepithelial lesions recognition in colposcopy images. *Scientific Reports*, 10(1): 1-12. <https://doi.org/10.1038/s41598-020-68252-3>
- [12] Priya, S., Karthikeyan, N.K. (2020). A heuristic and ANN based classification model for early screening of cervical cancer. *International Journal of Computational Intelligence Systems*, 13(1): 1092-1100. <https://doi.org/10.2991/ijcis.d.200730.003>
- [13] Dhawan, S., Singh, K., Arora, M. (2021). Cervix image classification for prognosis of cervical cancer using deep neural network with transfer learning. *EAI Endorsed Transactions on Pervasive Health and Technology*, 7(27): e5. <http://dx.doi.org/10.4108/eai.12-4-2021.169183>
- [14] Kuko, M., Pourhomayoun, M. (2020). Single and clustered cervical cell classification with ensemble and deep learning methods. *Information Systems Frontiers*, 22(5): 1039-1051. <https://doi.org/10.1007/s10796-020-10028-1>
- [15] Pramanik, R., Biswas, M., Sen, S., de Souza Júnior, L.A., Papa, J.P., Sarkar, R. (2022). A fuzzy distance-based ensemble of deep models for cervical cancer detection. *Computer Methods and Programs in Biomedicine*, 219: 106776. <https://doi.org/10.1016/j.cmpb.2022.106776>
- [16] Yu, Y., Ma, J., Zhao, W., Li, Z., Ding, S. (2021). MSCI: A multistate dataset for colposcopy image classification of cervical cancer screening. *International Journal of Medical Informatics*, 146: 104352. <https://doi.org/10.1016/j.ijmedinf.2020.104352>
- [17] Jia, A.D., Li, B.Z., Zhang, C.C. (2020). Detection of cervical cancer cells based on strong feature CNN-SVM network. *Neurocomputing*, 411: 112-127. <https://doi.org/10.1016/j.neucom.2020.06.006>
- [18] Şentürk, Z.K., Süleyman, U.Z.U.N. (2022). An improved deep learning based cervical cancer detection using a median filter based preprocessing. *Avrupa Bilim ve Teknoloji Dergisi*, 32: 50-58. <https://doi.org/10.31590/ejosat.1045538>
- [19] Hu, L., Bell, D., Antani, S., et al. (2019). An observational study of deep learning and automated evaluation of cervical images for cancer screening. *JNCI: Journal of the National Cancer Institute*, 111(9): 923-932. <https://doi.org/10.1093/jnci/djy225>
- [20] Adem, K., Kiliçarslan, S., Cömert, O. (2019). Classification and diagnosis of cervical cancer with stacked autoencoder and softmax classification. *Expert Systems with Applications*, 115: 557-564. <https://doi.org/10.1016/j.eswa.2018.08.050>
- [21] Chandran, V., Sumithra, M.G., Karthick, A., George, T., Deivakani, M., Elakkiya, B., Subramaniam, U., Manoharan, S. (2021). Diagnosis of cervical cancer based on ensemble deep learning network using colposcopy images. *BioMed Research International*, 2021: 5584004. <https://doi.org/10.1155/2021/5584004>
- [22] Chitra, B., Kumar, S.S. (2021). An optimized deep learning model using Mutation-based Atom Search Optimization algorithm for cervical cancer detection. *Soft Computing*, 25: 15363-15376. <https://doi.org/10.1007/s00500-021-06138-w>
- [23] Alyafeai, Z., Ghouti, L. (2020). A fully-automated deep learning pipeline for cervical cancer classification. *Expert Systems with Applications*, 141: 112951. <https://doi.org/10.1016/j.eswa.2019.112951>
- [24] Khamparia, A., Gupta, D., Rodrigues, J.J., de Albuquerque, V.H.C. (2021). DCAVN: Cervical cancer prediction and classification using deep convolutional and variational autoencoder network. *Multimedia Tools and Applications*, 80: 30399-30415. <https://doi.org/10.1007/s11042-020-09607-w>
- [25] Diniz, D.N., Rezende, M.T., Bianchi, A.G.C., Carneiro, C.M., Luz, E.J.S., Moreira, G.J.P., Ushizima, D.M., de Medeiros, F.N.S., Souza, M.J.F. (2021). A deep learning ensemble method to assist cytopathologists in pap test image classification. *Journal of Imaging*, 7(7): 111. <https://doi.org/10.3390/jimaging7070111>
- [26] Mohammed, M.A., Abdurahman, F., Ayalew, Y.A. (2021). Single-cell conventional pap smear image classification using pre-trained deep neural network architectures. *BMC Biomedical Engineering*, 3(1): 11. <https://doi.org/10.1186/s42490-021-00056-6>
- [27] Desiani, A., Suprihatin, B., Yahdin, S., Putri, A.I., Husein, F.R. (2021). Bi-path architecture of CNN segmentation and classification method for cervical cancer disorders based on pap-smear images. *IAENG International Journal of Computer Science*, 48(3).
- [28] Bhatt, A. R., Ganatra, A., Kotecha, K. (2021). Cervical cancer detection in pap smear whole slide images using convnet with transfer learning and progressive resizing. *PeerJ Computer Science*, 7: e348. <https://doi.org/10.7717/peerj-cs.348>
- [29] Shi, J., Wang, R., Zheng, Y., Jiang, Z., Yu, L. (2019). Graph convolutional networks for cervical cell classification. In MICCAI 2019 Computational Pathology Workshop COMPAY.
- [30] Talo, M. (2019). Diagnostic classification of cervical cell images from pap smear slides. *Academic Perspective Procedia*, 2(3): 1043-1050. <https://doi.org/10.33793/acperpro.02.03.116>
- [31] Win, K.P., Kitjaidure, Y., Hamamoto, K., Myo Aung, T. (2020). Computer-assisted screening for cervical cancer using digital image processing of pap smear images. *Applied Sciences*, 10(5): 1800. <https://doi.org/10.3390/app10051800>